Journal of Power Sources 196 (2011) 6022–6028

Contents lists available at ScienceDirect

Journal of Power Sources

journal homepage: www.elsevier.com/locate/jpowsour

Degradation mechanism of Ni-based anode in low concentrations of dry methane

Gang Chen [a,*], Guoqing Guan [b], Yutaka Kasai [c], Hong-Xin You [d], Abuliti Abudula [a,b,**]

[a] Graduate School of Science and Technology, Hirosaki University, 1-bunkyocho, Hirosaki 036-8560, Japan
[b] North Japan Research Institute for Sustainable Energy (NJRISE), Hirosaki University, 2-1-3 Matsubara, Aomori 030-0813, Japan
[c] Industrial Research Institute, Aomori Prefectural Industrial Technology Research Center, 4-11-6 Second Tonyamachi, Aomori 030-0113, Japan
[d] Chemical Engineering College, Dalian University of Technology, No. 2 Linggong Road, Dalian 116024, PR China

ARTICLE INFO

Article history:
Received 3 January 2011
Received in revised form 1 March 2011
Accepted 29 March 2011
Available online 12 April 2011

Keywords:
Solid oxide fuel cell
Degradation mechanism
Bimetallic anode
Ni
Re-oxidation
Methane

ABSTRACT

Degradation mechanism of $Ni_{0.5}Cu_{0.5}$–$Gd_{0.2}Ce_{0.8}O_{1.9}$ (CGO) bimetallic anode in low concentrations of dry methane is studied with a $(La_{0.75}Sr_{0.25})_{0.95}MnO_{3-\delta}$–CGO cathode supported SOFC. Leakage tests suggested that as-prepared cells are well-sealed by glass ring at elevated temperatures. OCV of as-prepared cell in each concentration of CH_4 is over 1.2 V, indicating that the ScSZ electrolyte film prepared by a dual drying pressing method is dense enough. It is found that rapid degradation phenomenon easily occurred at relatively high current density in 7.4 and 14.8% of dry methane in the performance test. XRD and EIS analyses indicated that the degradation of the $Ni_{0.5}Cu_{0.5}$–CGO anode at high current density could be mainly attributed to the re-oxidation of Ni. GC results showed that the re-oxidation of Ni always occurred at a relatively high $p(H_2O)$, which always appeared at a relatively high current density. The degraded cell is successfully recovered by burning the anode with O_2 and re-reducing with H_2.

1. Introduction

Solid oxide fuel cell (SOFC) operated by directly using hydrocarbon fuels without external reforming is expected to be an important device for energy generation in future [1,2]. The generally used SOFC anode materials such as Ni/YSZ usually show a number of disadvantages including Ni coarsening [3], sulfur poisoning [4–6], carbon deposition [7–11] and redox instability [12–15]. In order to overcome these disadvantages, several alternative materials have been developed as potential anodes in recent years [16–18]. Gorte et al. [19–23] solved the problem of carbon deposition by using a Cu–CeO_2 anode. It is possible that Cu is a poor catalyst for making and breaking C–C bonds, and it could prevent graphite formation [24]. Kim et al. [25] also demonstrated that carbon formation was greatly suppressed when Cu–Ni alloys were used. Sin et al. [26] found that NiCu–CGO anode had a good long-term stability when running in dry methane at 750 °C. However, the output voltage as well as the corresponding power density of the cell with NiCu–CGO anode decreased rapidly when the current density increased to a higher value in dry methane. You et al. [27] reported a similar phenomenon even when the Ni–ScSZ anode was operated in low concentration of dry methane. In order to understand the degradation mechanism, many researchers [28–30] usually studied the structural and dimensional change of the Ni-based anode, which resulted in the damage of the cell, through reducing and oxidizing Ni in hydrogen and oxygen repeatedly. However, the degradation mechanism of Ni-based anode is still unclear when it is performed at high current density. In this study, the rapid degradation phenomenon was observed at high current density in low concentration of methane by gradual loading of current in the performance test, and a better understanding of the degradation mechanism was achieved.

Compared with SOFCs using pure methane as fuel, those cells using low-concentration methane can generate the similar amount of power density but lead to little carbon deposition. In this case, it is possible to investigate the reaction as well as the degradation mechanism via analysis of the outlet gas compositions on the anode side since the effect of carbon deposition can be ignored. In this study, in order to understand the degradation mechanism of the Ni-based anodes in low concentrations of dry methane, $Ni_{0.5}Cu_{0.5}$–CGO bimetallic anode was fabricated on a 11 mol% Sc_2O_3-doped ZrO_2 (ScSZ) electrolyte film with a $(La_{0.75}Sr_{0.25})_{0.95}MnO_{3-\delta}$ (LSM) + CGO cathode substrate, and its performance was investigated in 7.4 and 14.8% of dry methane environment, respectively.

* Corresponding author.
Tel.: +81 17 735 3362; fax: +81 17 735 5411.
** Corresponding author at: North Japan Research Institute for Sustainable Energy (NJRISE), Hirosaki University, 2-1-3 Matsubara, Aomori 030-0813, Japan.
Tel.: +81 17 735 3362; fax: +81 17 735 5411.
E-mail addresses: chen_1721@hotmail.com (G. Chen), abuliti@cc.hirosaki-u.ac.jp (A. Abudula).

0378-7753/$ – see front matter © 2011 Elsevier B.V. All rights reserved.
doi:10.1016/j.jpowsour.2011.03.103

2. Experimental

2.1. Fabrication of unit-cells

$Ni_{0.5}Cu_{0.5}O$ powders were prepared by a glycine–nitrate combustion method as reported previously [31]. Commercial LSM (CAS, China), CGO (CAS, China) and starch powders in a weight ratio of 6:4:3.5 were first ball-milled in ethanol for 24 h and 5 wt% (relative to LSM + CGO) of polyvinyl butyral (PVB) was then added with ethanol. The obtained mixture was subsequently dried with agitation and ground with mortar and pestle, and the powder was then sieved through a 150 μm mesh sieve. The mixed powder was pressed under 30 MPa in a stainless-steel die in order to obtain the substrate. The ScSZ (Tosoh Corporation, Japan) powder with 5 wt% PVB (relative to ScSZ) was added onto the substrate and co-pressed at 200 MPa to form an assembly. In order to obtain a cell with better bending strength and a sufficiently dense electrolyte film, the assembly was subsequently sintered at 1300 °C for 8 h in air. The thickness of the electrolyte film was determined by the amount of ScSZ powder. The porosity of the cathode substrate was measured using a standard Archimedes method. $Ni_{0.5}Cu_{0.5}O$–CGO powders in a weight ratio of 6:4 were also ball-milled in ethanol for 24 h, and coated on the electrolyte as anode by a slurry coating method. Then, the as-prepared anode was sintered at 1000 °C in air for 3 h. For comparison, NiO–CGO anode in a weight ratio of 6:4 was prepared on the electrolyte and sintered at 1300 °C for 3 h. The effective area of the anode was 0.78 cm^2.

2.2. Measurement

As-prepared cells were tested in Norwegian Electro Ceramics AS (NorECs) SOFC performance testing rig, in which cell was sealed by a glass ring. It is found that the glass ring began to soften up, and the cell was able to be well sealed at a temperature above 750 °C. The performances of the cells with $Ni_{0.5}Cu_{0.5}O$–CGO anode were tested by changing the external current load in 7.4% and 14.8% of dry methane with Ar at different temperatures, respectively. The flow rate of different concentrations of methane with Ar was kept at 54 ml min^{-1}. The current collector was Pt mesh. The anode was reduced with hydrogen for 30 min prior to test. For comparison, a cell with NiO–CGO anode was tested in 10% of H_2 with Ar. The flow rate of O_2 for all tested cells was kept at 50 ml min^{-1}. The impedances were measured between 0.1 Hz and 1 MHz using a frequency response analyzer and a potentiostat (Solartron 1250B and 1286, respectively). The microstructure and morphology of the cell after testing were observed using scanning electron microscopy (SEM, Hitachi, S-800, Japan). To check the NiCu alloy phase after performance testing, X-ray diffraction (XRD, Shimadzu, Japan) with Cu Kα radiation was used. The anode outlet gases were analyzed online using the Agilent GC 7890A gas chromatography system. Each measurement was performed in 10 min as the current was changed. The current density in this study was calculated by current based on the anode area of 0.78 cm^2.

3. Results and discussion

Fig. 1 shows the performance testing results of the as-prepared cell with $Ni_{0.5}Cu_{0.5}$–CGO anode at 800 °C. Firstly, the anode was reduced in 100 ml min^{-1} of H_2, while 100 ml min^{-1} of O_2 flowed on the cathode side simultaneously. The open-circuit voltage (OCV) was 1.242 V in process I in a stable state, indicating that the cell was well-sealed and the ScSZ electrolyte film prepared by dual dry pressing method was sufficiently dense. Then the cell was tested in 7.4% of dry methane, and a value of 1.305 V for the OCV was obtained. As indicated in process II of Fig. 1, the output voltage

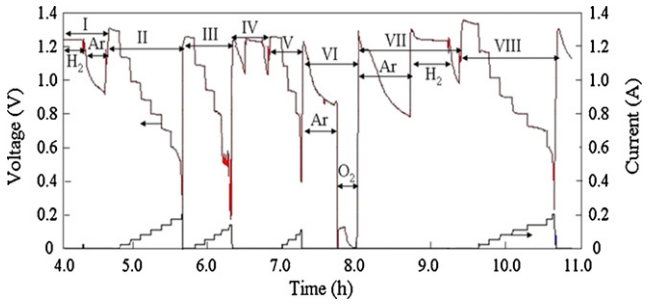

Fig. 1. Performance testing process of the cell with $Ni_{0.5}Cu_{0.5}$–CGO anode in 7.4% of dry methane at 800 °C (I. H_2 reduction and Ar purging; II. performance testing; III. performance testing after degradation; IV. second H_2 reduction and Ar purging; V. performance testing after second H_2 reduction; VI. Ar purging and O_2 burning; VII. Ar purging and H_2 reduction; VIII. performance testing after performance recovered).

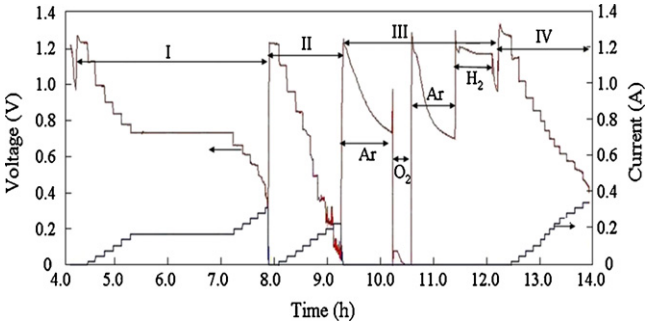

Fig. 2. Performance testing process of the cell with $Ni_{0.5}Cu_{0.5}$–CGO anode in 14.8% of dry methane at 850 °C (I. performance testing; II. performance testing after degradation; III. Ar purging, O_2 burning, Ar purging and H_2 reduction; IV. performance testing after performance recovered).

of the cell in 7.4% of dry methane kept unchanged during the test period if the current density in the cell circuit was set to a value below 0.18 A cm^{-2}. However, the output voltage of the cell began to decline with the test time at 0.18 A cm^{-2}, and rapidly declined at 0.218 A cm^{-2}. The same phenomenon was also observed when the $Ni_{0.5}Cu_{0.5}$–CGO anode was operated in 14.8% of dry methane at 850 °C (as indicated in process I of Fig. 2) and when the Ni–CGO anode worked in 10% of H_2 at 800 °C (as indicated in process I of Fig. 3). As indicated in process I of Fig. 2, no obvious degradation was observed when the $Ni_{0.5}Cu_{0.5}$–CGO anode was tested at 0.218 A cm^{-2} for 2 h in 14.8% of dry methane at 850 °C. However, the output voltage began to decline with the test time at 0.333 A cm^{-2}, and rapidly declined at 0.41 A cm^{-2} in process I of Fig. 2. As shown in Fig. 4, after being tested in 14.8% of dry methane at 850 °C for 11 h, almost no degradation was observed in the $Ni_{0.5}Cu_{0.5}$–CGO

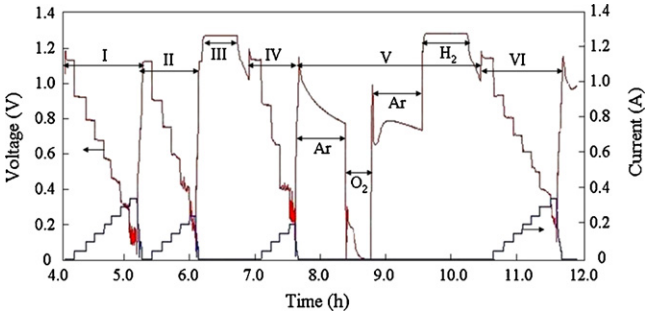

Fig. 3. Performance testing process of the cell with Ni–CGO anode in 10% of H_2 at 800 °C (I. performance testing; II. performance testing after degradation; III. second H_2 reduction; IV. performance testing after second H_2 reduction; V. Ar purging, O_2 burning, Ar purging and H_2 reduction; VI. performance testing after recovered).

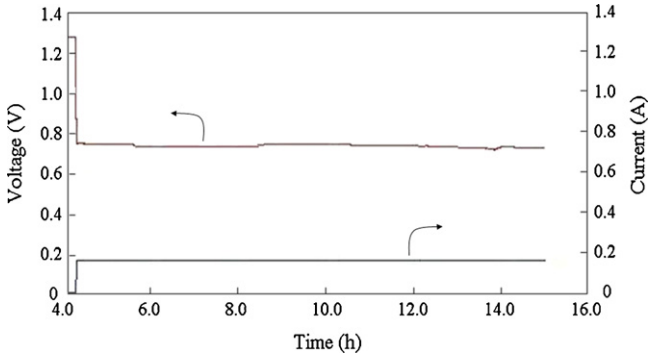

Fig. 4. 11 h stability test of $Ni_{0.5}Cu_{0.5}$–CGO anode in 14.8% of dry methane at 850 °C (current density maintained at 0.218 A cm^{-2}).

anode cell when it worked at 0.218 A cm^{-2}. The same rapid degradation phenomenon at the Ni–CGO anode in 10% of H_2 as in 14.8% of dry methane and the long time stability of the $Ni_{0.5}Cu_{0.5}$–CGO anode in 14.8% of dry methane at low current densities indicated that the rapid degradation of the $Ni_{0.5}Cu_{0.5}$–CGO anode at high current density was not predominantly caused by carbon deposition. The performance at each current density in process III of Fig. 1 was lower than that of the previous process, and the output voltage as well as the corresponding power density still decreased rapidly at a higher current density. The OCV of process III of Fig. 1 also dropped to 1.257 V, indicating that the performance of the cell degraded. The same phenomenon was also observed in process II of Fig. 2 with 14.8% of dry methane as fuel on the $Ni_{0.5}Cu_{0.5}$–CGO anode and in process II of Fig. 3 with 10% of H_2 as fuel on the Ni–CGO anode. After the cells were reduced in H_2 for 20 min in process IV of Fig. 1 and 30 min in process III of Fig. 3, the performances of the cell were unable to recover (as indicated in process V of Fig. 1 and process IV of Fig. 3). In process VI of Fig. 1, both fuel and O_2 were firstly replaced by Ar until no fuel was detected by GC. O_2 was introduced into the anode side for 20 min to re-oxidize the anode, and then, the anode side was purged by Ar for approximately 40 min until no O_2 was detected. As indicated in processes VI and VII in Fig. 1, during the purging process for anode and cathode, the output voltage decreased gradually, indicating that the fuel and the O_2 was replaced by Ar gradually. Thereafter, the anode was reduced by H_2 for 30 min (as indicated in process VII of Fig. 1). As a result, the performance of the cell was successfully recovered (as indicated in process VIII of Fig. 1) and the OCV was increased to 1.325 V in process VIII of Fig. 1. The same phenomenon was also found in Figs. 2 and 3.

Fig. 5 shows typical *I–V* curves of the cell in (a) 7.4% of dry methane and in (b) 14.8% of dry methane at different processes. As shown in Fig. 5(a), the OCVs of the cell were 1.305, 1.257, 1.258 and 1.325 V at processes II, III, V and VIII, respectively. The corresponding peak power densities were 0.134, 0.082, 0.079 and 0.136 W cm^{-2}, respectively. As shown in Fig. 5(a), the OCVs of the cell at processes III and V were a little lower than those at processes II and VIII. The same phenomenon was found in Fig. 5(b), the OCV of the cell after degradation (1.225 V at process II) was lower than that at first testing (1.245 V at process I) and that after performance recovered (1.27 V at process IV). In general, each reaction related to

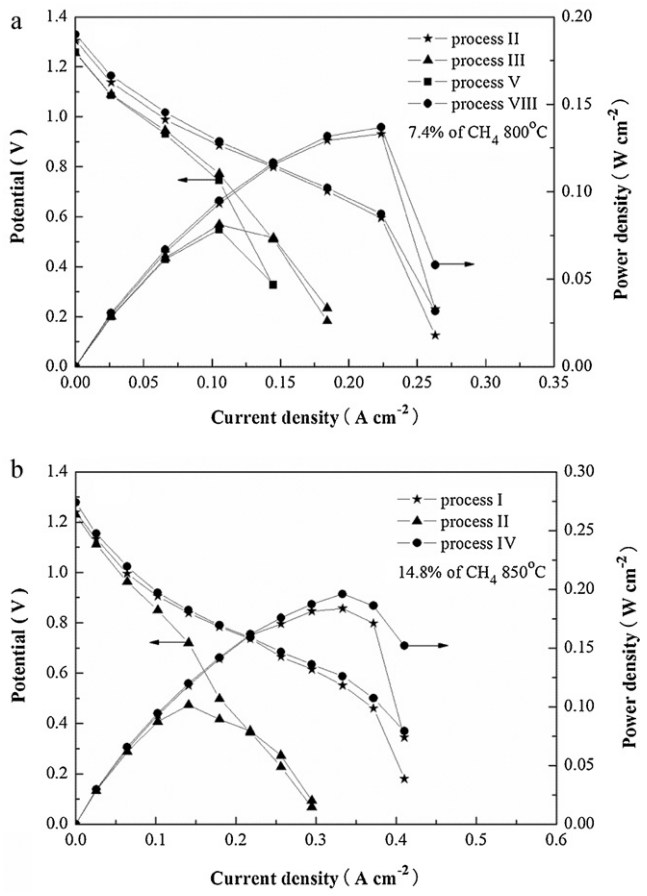

Fig. 5. Typical *I–V* curves of the cell in 7.4% of dry methane (a) and in 14.8% of dry methane (b) at different processes.

CH_4 at anode side can be expressed as

$$aA + bB \leftrightarrow cC + dD \quad (1)$$

and the corresponding Nernst equation for the OCV is

$$E = E^{\theta} - \frac{RT}{zF} \ln \left[\frac{(P_C/P_0)^c (P_D/P_0)^d}{(P_A/P_0)^a (P_B/P_0)^b} \right] \quad (2)$$

where A and B are CH_4 and O_2. C and D may be H_2 and CO due to partial electrochemical oxidation of methane (POM), or H_2O and CO_2 due to complete oxidation of methane (COM). P_0 is the standard atmospheric pressure. E^{θ} is the standard electromotive force.

Table 1 shows the partial pressures of CH_4, H_2, CO and CO_2 of the cell in 7.4% of dry methane at the anode side under open circuit condition at different processes. P_{anode} is absolute pressure of the anode chamber, $p(CH_4)$, $p(H_2)$, $p(CO)$ and $p(CO_2)$ are the partial pressures of CH_4, H_2, CO and CO_2 at the anode side, respectively. The presence of CO and slight CO_2 at open circuit condition might be due to the minor O^{2-} transported from the cathode because a small oxygen ion current may exist in circuit. In this study, a mixed ionic–electronic conductor, NiCu–CGO, was used as the anode. Huang and Huang [32,33] found that a phenomenon of electrochemical promotion of lattice-oxygen extraction from CGO bulk occurred during direct methane oxidation to generate syngas at

Table 1
Partial pressures of CH_4, H_2, CO and CO_2 of the cell in 7.4% of dry methane at the anode side under open circuit condition at different processes.

Process	$p(CH_4)/P_{anode}$ ($\times 10^2$)	$p(H_2)/P_{anode}$ ($\times 10^2$)	$p(CO)/P_{anode}$ ($\times 10^3$)	$p(CO_2)/P_{anode}$ ($\times 10^5$)
II	6.37	2.76	4.02	3.23
III	7.04	1.39	3.7	6.23

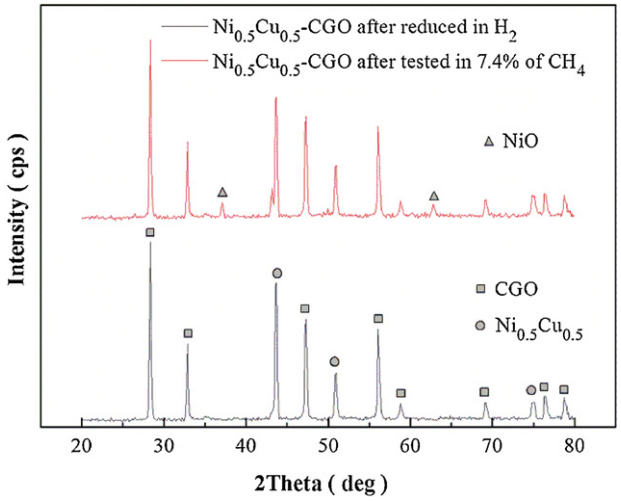

Fig. 6. XRD patterns of the $Ni_{0.5}Cu_{0.5}$–CGO cermets after reduced in H_2 and after tested in 7.4% of dry methane.

800 °C, even in the absence of anode-side gas-phase oxygen at the open circuit conditions. In the present situation, the similar phenomenon should be happened. The standard electromotive force of POM and COM calculated by Zhang et al. [34] with the Nernst equation were 1.228 V and 1.055 V at 800 °C, respectively, indicating that the E^{θ} of the POM is higher than that of the COM at 800 °C. As indicated in Table 1, the partial pressures of CO and H_2 decreased while the corresponding partial pressure of CO_2 increased in process III of Fig. 1, indicating that the COM in 7.4% of methane under open circuit after degradation increased, and the corresponding POM decreased. It may be the reason why the OCV decreased after degradation.

Fig. 6 shows the XRD patterns of the $Ni_{0.5}Cu_{0.5}$–CGO cermets after reduction in H_2 and after testing in 7.4% of dry methane. After reduction in H_2, the XRD of $Ni_{0.5}Cu_{0.5}$–CGO cermets exhibited a well-cubic fluorite structure and a good $Ni_{0.5}Cu_{0.5}$ alloy phase. However, NiO was found to be formed in $Ni_{0.5}Cu_{0.5}$–CGO cermets after being tested in 7.4% of dry methane. Thus, it is reasonable to deduce that re-oxidation of Ni occurred at high current density in low concentration of dry methane. As indicated above, the ScSZ layer is sufficiently dense to prohibit crossover of gases through the layer and the cell was well sealed. In this situation, the Ni could be oxidized by H_2O molecules generated from methane oxidation reactions and/or by oxygen ions transported from cathode side. In this case, more O^{2-} ions could transfer to the interface of electrolyte and anode at higher current densities. If no enough fuel reached the interface and reacted with the O^{2-}, Ni near the interface of electrolyte and anode could be also oxidized by O^{2-}. This could easily occur at the conditions when low concentrations of methane were used as fuel. As indicated in process IV of Fig. 1, it should be noted that NiO formed at high current density seemed to be unable to be reduced if the degraded anode was reduced directly in pure H_2. However, Ni re-oxidized by oxygen could be easily reduced by hydrogen [35–38], indicate that the NiO in this case might mainly from Ni re-oxidized by H_2O. As indicated in Figs. 1 and 2, after the anode was burnt in O_2 and then reduced in H_2, the performance of the cell was successfully recovered. It suggested that the oxidized Ni in the present case could be reduced by H_2 unless it was burnt in O_2 at first. Interestingly, as indicated in Fig. 3, the same phenomenon was also observed at the Ni–CGO anode in 10% of H_2. This indicated that the burning in O_2 not only served to remove possibly deposited carbon when low concentration of methane was used as fuel, but also might remove some other chemicals such as H_2O molecules or hydroxyl deposited on NiO. As indicated by Schulze et al. [39], H_2O molecules could form a monolayer coverage on NiO at high temperatures so that NiO formed by oxidization of Ni in water vapor cannot be reduced in H_2 before treatment with O_2 [40].

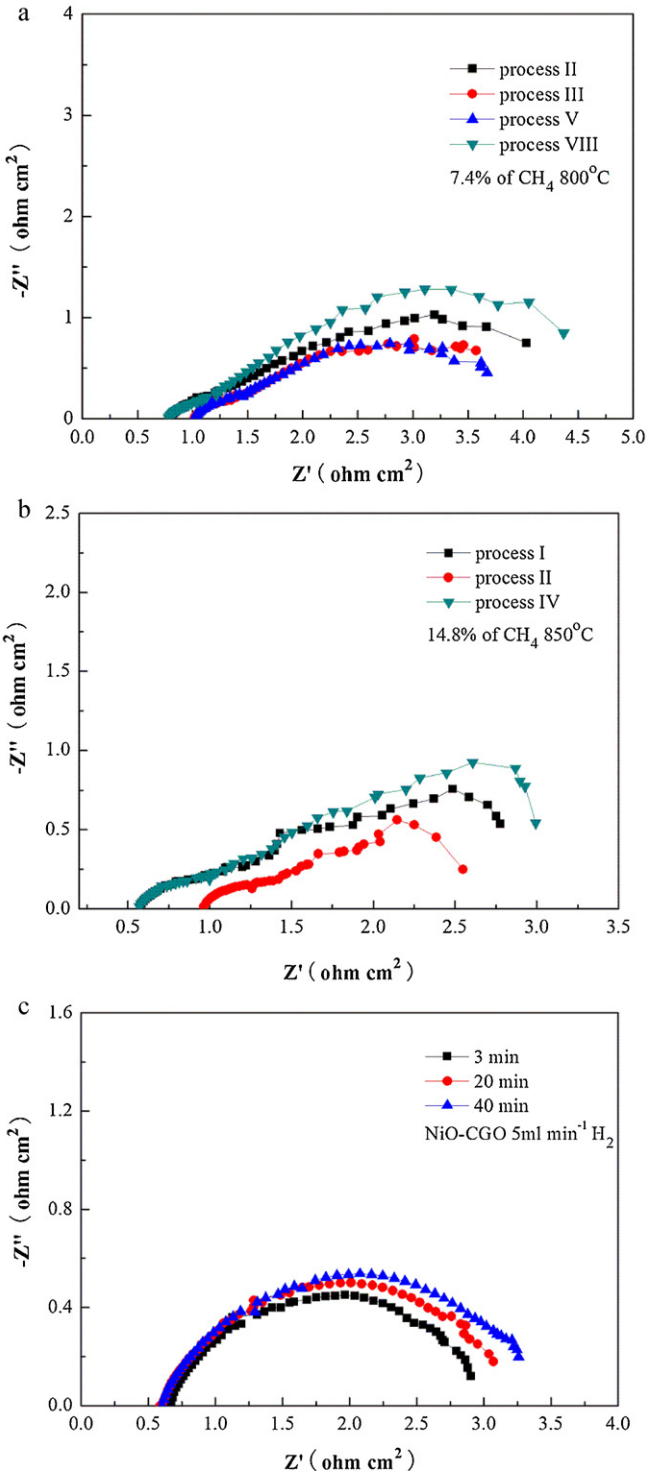

Fig. 7. Impedance spectra of the NiCu–CGO anode cells in 7.4% of dry methane (a) and in 14.8% of dry methane (b) at different processes under open circuit condition; (c) impedance spectra of the NiO–CGO anode cell reduced in 5 ml min^{-1} H_2 at 800 °C for different periods under open circuit condition.

Fig. 7(a) and (b) shows the impedance spectroscopy measured under open circuit condition at the different processes shown in Figs. 1 and 2, respectively. The ac impedance is made up of both ohmic and electrode polarization resistances. The low frequency

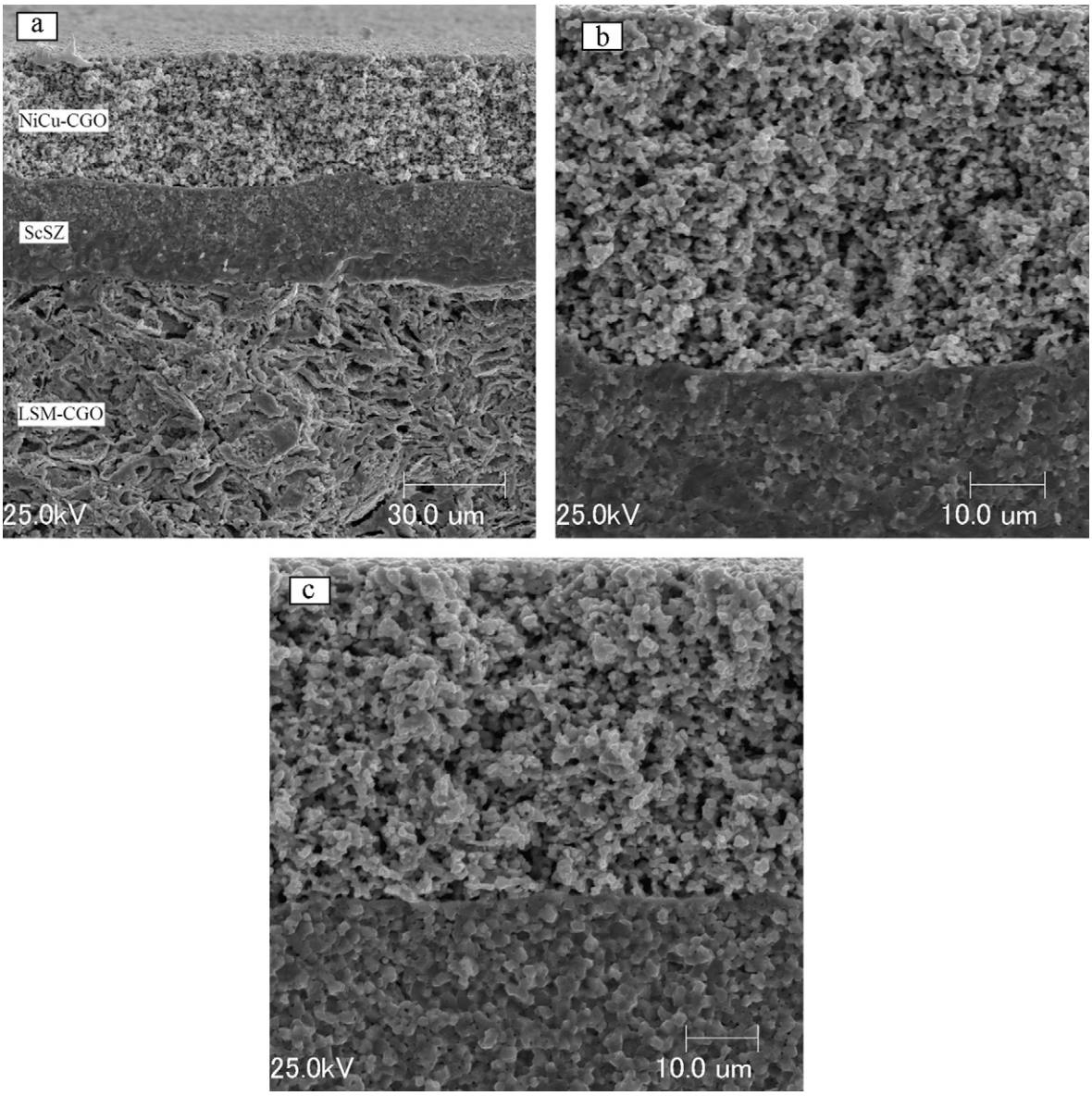

Fig. 8. Cross-section of the cell: (a) overview of the sandwich structure of the whole cell after degradation, (b) high magnification of the anode and electrolyte without degradation and (c) high magnification of the anode and electrolyte after degradation.

intercept corresponds to the total resistance of the cell. The high frequency intercept represents the ohmic resistance (R_o), involving ionic resistance of the electrolyte, electronic resistance of the electrodes, and some contact resistance associated with interfaces. The difference between the high and low frequency intercepts represents the electrode polarization resistance (R_p) [41]. As shown in Fig. 7(a), the R_o values of the cell tested in 7.4% of dry methane were 0.8, 1.02, 1.017 and 0.78 $\Omega\,cm^2$ at processes II, III, V and VIII, respectively. The higher R_o shown in process II of Fig. 7(b) and in processes III and V of Fig. 7(a) also indicate that some new materials such as NiO with low electronic conductivity could be formed after performance degradation. Furthermore, the R_p of the cell tested in 7.4% of methane at processes III and V were smaller than those at processes II and VIII in Fig. 7(a) while the R_p of the cell tested in 14.8% of methane at process II was smaller than those at processes I and IV in Fig. 7(b), indicating that the R_p of the cell after degradation was lower than that of the cell without degradation. The same phenomenon was also found in Fig. 7(c), which shows impedance spectra of the NiO–CGO anode cell reduced in 5 ml min^{-1} H_2 for different periods at 800 °C. As shown in Fig. 7(c), the R_o of the cell after 3 min reduction was a little higher than those after 20 and 40 min reductions, but the R_p after 3 min reduction was obviously lower than those after 20 and 40 min reductions. It indicated that NiO could not be completely reduced in H_2 flowing for 3 min. The higher R_p for 3 min reduction cell in Fig. 7(c) confirmed that the rapid degradation at the NiCu–CGO anode in 7.4 and 14.8% of dry methane was also mainly induced by re-oxidation of Ni. The reason for the lower Rp in the anode with the existence of NiO may be the decreasing of activation polarization with the decrease in active Ni. Sumi et al. [42] indicated that the R_p of Ni–YSZ anode in a supply of H_2–CO–CO_2 mixtures increased with the increase in CO concentration at 1023 K because of the difficulty of electrochemical oxidation of carbon monoxide. In our case, as indicated in Table 1, the concentrations of H_2 and CO at open circuit condition after degradation (process III) were lower than those of first testing (process II), also indicated that the concentration of CO had great effect on R_p. On the other hand, Sumi et al. [42] also showed that the R_p of the cell in the existence of H_2O in methane was smaller than that in the case without H_2O for both of the Ni–YSZ and Ni–ScSZ anodes at 1273 K, indicating that H_2O had great effect on R_p. As

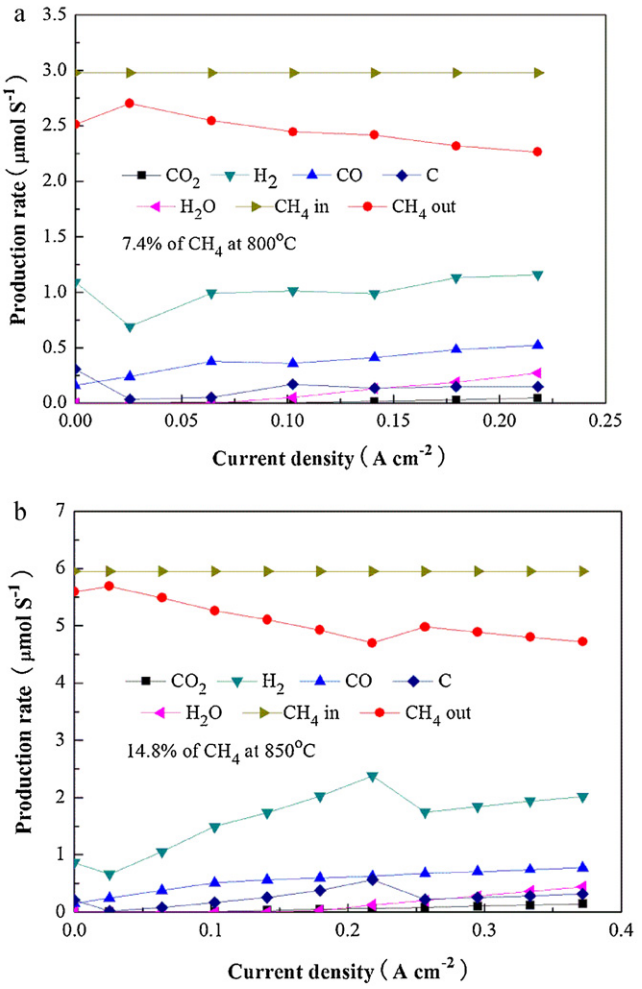

Fig. 9. Production rates of the anodic exhausts for SOFCs with 7.4% of methane (a) and with 14.8% of methane (b) corresponding to the process II of Fig. 1 and process I of Fig. 2, respectively.

indicated above, H_2O monolayer could cover NiO after performance degradation.

Fig. 8(a) shows the cross-sectional SEM of the sandwich structure of the whole cell. The thickness of the cathode substrate, anode and electrolyte were about 680, 40 and 32 μm, respectively. Some isolated defects such as small voids were observed in the electrolyte film. However, no cross-membrane cracks or pinholes were observed. The OCVs of the cell were as high as 1.242 and 1.305 V at 800 °C in hydrogen and 7.4% of dry methane, respectively, which proved that the ScSZ layer was sufficiently dense to prohibit crossover of gases through the layer. The electrodes showed a typical porous microstructure. Porosity of the cathode substrate was about 38% as determined by the Archimedes method in water. As indicated in Ref. [43], the phase change from Ni to NiO involved a volumetric expansion of 69%, which resulted in a dimensional expansion of the anode. It was found that the electrolyte on an anode-supported SOFC was cracked after several redox cyclings [12]. However, as shown in Fig. 8(a) and (b), for our cells, no crack was observed in the electrolyte and anode, indicating that cracking of electrolyte induced by redox cycling of anode could be avoided in cathode-supported type SOFC. The minimal difference between Fig. 8(b) and (c) suggested that only a little Ni could be re-oxidized by H_2O in this case.

Fig. 9(a) and (b) shows the production rates of anode outlet gases for 7.4% of methane at 800 °C and 14.8% of methane at 850 °C, which correspond to the process II in Fig. 1 and process I in Fig. 2, respectively. The production rates of CO_2, CO and $(CH_4)_{out}$ were calculated based on GC measurements. Production rates of H_2O, H_2 and carbon deposition rate were calculated by elements equilibrium based on the inlet flux of CH_4 and the amount of O^{2-} transported from cathode to anode. As indicated above, the ScSZ layer was sufficiently dense to prohibit crossover of gases through the layer and the cell was well sealed in the process of performance testing. The amount of O^{2-} transported from cathode to anode should be controlled by the loaded current.

The production rate of carbon deposition, H_2O and H_2 were calculated in sequence by carbon balance, oxygen balance and hydrogen balance.

$$\nu(C)_{dep} = \nu(CH_4)_{in} - \nu(CH_4)_{out} - \nu(CO)_{out} - \nu(CO_2)_{out} \quad (3)$$

$$\nu(O^{2-}) = I/2F \quad (4)$$

$$\nu(H_2O)_{fO} = \nu(O^{2-}) - \nu(CO)_{out} - 2\nu(CO_2)_{out} \quad (5)$$

$$\nu(H_2)_{fH} = 2[\nu(CH_4)_{in} - \nu(CH_4)_{out}] - \nu(H_2O)_{out} \quad (6)$$

where $\nu(C)_{dep}$ is carbon deposition rate, $\nu(CH_4)_{in}$ is the inlet flux of CH_4, $\nu(CH_4)_{out}$, $\nu(CO)_{out}$, $\nu(CO_2)_{out}$ and $\nu(H_2)_{fH}$ are the outlet fluxes of CH_4, CO, CO_2, and H_2, respectively. In Eq. (4), the $\nu(O^{2-})$ is the O^{2-} flux calculated from the current (I) passing though the electrolyte where F is the Faraday constant. As shown in Fig. 9(a) and (b), at a low current density (low oxygen stoichiometry) with open circuit condition, only a little amount of CO_2 and H_2O could be generated, indicating that the POM dominated the methane reactions at low-current density. As the current increased (the amount of O^{2-} transported from cathode to anode increased), the amount of H_2O began to increase. Previous work of our group demonstrated that the current density of electrochemical methane oxidation reactions increases in the following order [27]:

$$CH_4 + O^{2-} \rightarrow CO + 2H_2 + 2e^- \quad (7)$$

$$CH_4 + 2O^{2-} \rightarrow CO + H_2O + H_2 + 4e^- \quad (8)$$

$$CH_4 + 3O^{2-} \rightarrow CO + 2H_2O + 6e^- \quad (9)$$

$$CH_4 + 4O^{2-} \rightarrow CO_2 + 2H_2O + 8e^- \quad (10)$$

According to Eqs. (7)–(10), it is easy to understand that the production rates of H_2O increase linearly with current density. On the other hand, the only product of Ni–CGO anode SOFC with H_2 as fuel in Fig. 3 was H_2O. It is obvious that the production rate of H_2O increased with the decrease in the amount of H_2 at outlet as current density increased. Thus, higher current density resulted in a higher $p(H_2O)$. As reported in some Refs. [40,44,45] Ni could be re-oxidized by the produced H_2O with a high partial pressure when the fuel was greatly utilized. In the present case, more H_2O was formed at a higher current density in 7.4 and 14.8% of dry methane in the process II of Fig. 1 and process I of Fig. 2, respectively, leading to a higher $p(H_2O)$. As a result, Ni could be oxidized by the produced H_2O at a high current density, and the output voltage as well as the corresponding power density decreased rapidly.

4. Conclusions

Cathode-supported SOFC consisting of a $Ni_{0.5}Cu_{0.5}$–CGO anode with a ScSZ electrolyte on a LSM–CGO cathode substrate was fabricated via a dual drying pressing followed by co-firing method. The rapid degradation mechanism of $Ni_{0.5}Cu_{0.5}$–CGO anode at high current density in low concentrations of dry methane was studied in the case of well-seal state. XRD and EIS analyses indicated that Ni re-oxidation easily occurred at a relatively high current density in low concentrations of dry methane. GC results indicated that the relatively high $p(H_2O)$ obtained at a high current density could

be the main reason for the performance degradation of Ni-based anode in low concentrations of methane. Ni in the anode could be oxidized by H_2O molecules in the present case. The re-oxidized Ni was able to be reduced in H_2 unless it was re-oxidized again in O_2 before the reduction.

Acknowledgements

This study was supported by the Go Go Foundation of Hirosaki University and by the State Scholarship Fund of China Scholarship Council (2008).

References

[1] M.D. Gross, J.M. Vohs, R.J. Gorte, Electrochim. Acta 52 (2007) 1951–1957.
[2] Y. Nabae, I. Yamanaka, M. Hatano, K. Otsuka, J. Electrochem. Soc. 153 (1) (2006) A140–A145.
[3] A. Atkinson, S. Barnett, R.J. Gorte, J.T.S. Irvine, A.J. Mcevoy, M. Mogensen, S.C. Singhal, J. Vohs, Nat. Mater. 3 (2004) 17–27.
[4] A. Lussier, S. Sofie, J. Dvorak, Y.U. Idzerd, Int. J. Hydrogen Energy 33 (2008) 3945–3951.
[5] J.H. Wang, M.L. Liu, J. Power Sources 176 (2008) 23–30.
[6] C.M. Grgicak, R.G. Green, J.B. Giorgi, J. Power Sources 179 (2008) 317–328.
[7] H. Kan, H. Lee, Appl. Catal. B: Environ. 97 (2010) 108–114.
[8] C.M. Finnerty, N.J. Coe, R.H. Cunningham, R.M. Ormerod, Catal. Today 46 (1998) 137–145.
[9] K. Nikooyeh, R. Clemmer, V. Alzate-Restrepo, J.M. Hill, Appl. Catal. A: Gen. 347 (2008) 106–111.
[10] N.C. Triantafyllopoulos, S.G. Neophytides, J. Catal. 217 (2003) 324–333.
[11] N.C. Triantafyllopoulos, S.G. Neophytides, J. Catal. 239 (2006) 187–199.
[12] D. Waldbillig, A. Wood, D.G. Ivey, J. Power Sources 145 (2005) 206–215.
[13] Y. Zhang, B. Liu, B.F. Tu, Y.L. Dong, M.J. Cheng, Solid State Ionics 176 (2005) 2193–2199.
[14] Y.H. Heo, J.W. Lee, S.B. Lee, T.H. Lim, S.J. Park, R.H. Song, C.O. Park, D.R. Shin, Int. J. Hydrogen Energy 36 (2011) 797–804.
[15] B. Iwanschitz, J. Sfeir, A. Mai, M. Schützeb, J. Electrochem. Soc. 157 (2) (2010) B269–B278.
[16] S.W. Tao, J.S. Irvine, Nat. Mater. 2 (2003) 320–323.
[17] S.W. Tao, J.T.S. Irvine, Chem. Rec. 4 (2004) 83–95.
[18] B.A. Boukamp, Nat. Mater. 2 (2003) 294–296.
[19] C. Lu, W.L. Worrell, J.M. Vohs, R.J. Gorte, J. Electrochem. Soc. 150 (2003) A1357–A1359.
[20] S. An, C. Lu, W.L. Worrell, R.J. Gorte, J.M. Vohs, Solid State Ionics 175 (2004) 135–138.
[21] R.J. Gorte, S. Park, J.M. Vohs, C.-H. Wang, Adv. Mater. 12 (2000) 1465–1469.
[22] O. Costa-Nunes, R.J. Gorte, J.M. Vohs, J. Power Sources 141 (2005) 241–249.
[23] R.J. Gorte, J.M. Vohs, J. Catal. 216 (2003) 477–486.
[24] X.-F. Ye, S.R. Wang, Z.R. Wang, L. Xiong, X.F. Sun, T.L. Wen, J. Power Sources 177 (2008) 419–425.
[25] H. Kim, C. Lu, W.L. Worrell, J.M. Vohs, R.J. Gorte, J. Electrochem. Soc. 149 (3) (2002) A247–A250.
[26] A. Sin, E. Kopnin, Y. Dubitsky, A. Zaopo, A.S. Aricò, D. La Rosa, L.R. Gullo, V. Antonucci, J. Power Sources 164 (2007) 300–305.
[27] H.-X. You, H.J. Gao, G. Chen, A. Abudula, X.W. Ding, J. Power Sources 196 (2011) 2779–2784.
[28] M. Ettler, H. Timmermann, J. Malzbender, A. Weber, N.H. Menzler, J. Power Sources 195 (2010) 5452–5467.
[29] J. Laurencin, G. Delette, B. Morel, F. Lefebvre-Joud, M. Dupeux, J. Power Sources 192 (2009) 344–352.
[30] Q. Jeangros, A. Faes, J.B. Wagner, T.W. Hansen, U. Aschauer, J. Van herle, A. Hessler-Wyser, R.E. Dunin-Borkowski, Acta Mater. 58 (2010) 4578–4589.
[31] Z. Xie, R.C. Xia, M.Y. Zhang, W. Zhu, H.T. Wang, J. Power Sources 161 (2006) 1056–1061.
[32] T.J. Huang, M.C. Huang, Chem. Eng. J. 138 (2007) 538–547.
[33] T.J. Huang, M.C. Huang, J. Power Sources 168 (2007) 229–235.
[34] X. Zhang, S. Ohara, H. Chen, T Fukui, Fuel 81 (2002) 989–996.
[35] T. Klemenso, C.C. Appel, M. Mogensen, Solid State Lett. 9 (2006) A403–A407.
[36] T. Klemenso, C. Chung, P.H. Larsen, M. Mogensen, J. Electrochem. Soc. 152 (2005) A2186–A2192.
[37] D. Waldbillig, A. Wood, D.G. Ivey, Solid State Ionics 176 (2005) 847–859.
[38] J. Malzbender, E. Wessel, R.W. Steinbrech, Solid State Ionics 176 (2005) 2201–2203.
[39] M. Schulze, R. Reissner, M. Lorenz, U. Radke, W. Schnurnberger, Electrochim. Acta 44 (1999) 3969–3976.
[40] M. Lorenz, M. Schulze, Surf. Sci. 454–456 (2000) 234–239.
[41] C. Zhao, R.Z. Liu, S.R. Wang, Z. Wang, J. Qian, T.L. Wen, J. Power Sources 192 (2009) 552–555.
[42] H. Sumi, Y.H. Lee, H. Muroyama, T. Matsui, K. Eguchi, J. Electrochem. Soc. 157 (8) (2010) B1118–B1125.
[43] M. Pihlatie, A. Kaiser, M. Mogensen, Solid State Ionics 180 (2009) 1100–1112.
[44] D. Sarantaridis, A. Atkinson, Fuel Cells 7 (2007) 246–258.
[45] Q. Ma, F. Tietz, A. Leonide, E. Ivers-Tiffée, Electrochem. Comm. 12 (2010) 1326–1328.